Physics of the Earth and Planetary Interiors xxx (2014) xxx–xxx

Contents lists available at ScienceDirect

Physics of the Earth and Planetary Interiors

journal homepage: www.elsevier.com/locate/pepi

# Spin transition, substitution, and partitioning of iron in lower mantle minerals

Kiyoshi Fujino [a,*], Daisuke Nishio-Hamane [b], Takaya Nagai [c], Yusuke Seto [d], Yasuhiro Kuwayama [a], Matthew Whitaker [a,e], Hiroaki Ohfuji [a], Toru Shinmei [a], Tetsuo Irifune [a,f]

[a] Geodynamics Research Center, Ehime University, Matsuyama 790-8577, Japan
[b] Institute for Solid State Physics, University of Tokyo, Kashiwa 277-8581, Japan
[c] Department of Natural History Sciences, Hokkaido University, Sapporo 060-0810, Japan
[d] Department of Earth and Planetary Sciences, Kobe University, Kobe 657-8501, Japan
[e] Mineral Physics Institute, Stony Brook University, Stony Brook, NY 11794-2100, USA
[f] Earth-Life Science Institute, Tokyo Institute of Technology, Tokyo 152-8550, Japan

ARTICLE INFO

*Article history:*
Available online xxxx
Edited by Prof. M. Jellinek

*Keywords:*
Lower mantle
Spin transition of iron
Mg-perovskite
Post-Mg-perovskite
$Fe^{3+}$-Al coupled substitution
Iron-partitioning

ABSTRACT

Spin transition and substitution of $Fe^{3+}$ in $Fe^{3+}AlO_3$-bearing $MgSiO_3$ perovskite (Pv) and post-perovskite (PPv) were examined up to 200 and 165 GPa, respectively, at room temperature by X-ray emission spectroscopy (XES) and XRD. The results of XES and XRD indicate that in Pv high spin (HS) $Fe^{3+}$ at the dodecahedral (A) site replaces Al at the octahedral (B) site and becomes low spin (LS) between 50 and 70 GPa with pressure, while in PPv LS $Fe^{3+}$ occupies the B-site and Al occupies the A-site above 80–100 GPa. The $Fe^{3+}$–Al coupled substitution seems to be at work in both Pv and PPv. Combining these results on $Fe^{3+}$ with the recent first-principles calculations on $Fe^{2+}$ in Pv and PPv, the spin transition and substitution of iron in pyrolitic lower mantle minerals are proposed. Further, their effects on iron-partitioning among the lower mantle minerals are discussed.



## 1. Introduction

The major iron-bearing minerals in the lower mantle are generally believed to be Mg-perovskite (Pv) and ferropericlase (Fp) between 670 and 2600 km, and post-Mg-perovskite (PPv) and Fp between 2600 and 2900 km for pyrolitic mantle (Murakami et al., 2004), although the depth region where Pv and PPv coexist is not well constrained (Catalli et al., 2010b; Andrault et al., 2010). Recent experimental and theoretical studies on spin transition of iron indicate that pressure-induced high spin (HS) – low spin (LS) transitions of iron in lower mantle minerals strongly affect the structures and physical properties of minerals and thereby the dynamics of the lower mantle. However, spin transitions of iron in lower mantle minerals, with the exception of Fp, had been unclear. Particularly, there had been large discrepancies among the previous reports on spin transition of both $Fe^{2+}$ and $Fe^{3+}$ in Pv. The most conflicting point with $Fe^{2+}$ in Pv had been about the exsistence of intermediate spin (IS) or LS state of $Fe^{2+}$ at the lower mantle conditions (Badro et al., 2004; Jackson et al., 2005; Zhang and Oganov, 2006; Li et al., 2006; Stackhouse et al., 2007; McCammon et al., 2008, 2010; Lin et al., 2008). With this problem, the recent first-principles calculations clarified that the high quadrupole splitting (QS) of $Fe^{2+}$ in Mössbauer spectra, which had been often used as the evidence of the IS or LS state, should be assigned to the HS state of $Fe^{2+}$ at high pressure, and the HS state of $Fe^{2+}$ remains stable at the lower mante conditions (Bengtson et al., 2009; Hsu et al., 2010, 2011). From these results, the spin state of $Fe^{2+}$ in Pv at the lower mantle conditions seems to have been settled as HS. However, with the spin state of $Fe^{3+}$ in Pv, the different spin states have been reported for the samples with similar compositions at the similar pressure and temperature conditions (Jackson et al., 2005; Li et al., 2005; Li et al., 2006; Zhang and Oganov, 2006; Stackhouse et al., 2007; Catalli et al., 2010a), and the large conflicts of the spin transition problems of $Fe^{3+}$ seem to still remain. Meanwhile, in contrast to the abundant reports on Pv, reports on spin transition of iron in PPv are very limited (Zhang and Oganov, 2006; Lin et al., 2008; Jackson et al., 2009; Catalli et al., 2010b; Yu et al., 2012).

In an attempt to resolve these situations and construct a more firm base for understanding the spin transition behaviors of iron in lower mantle minerals, we have examined the spin transitions of $Fe^{3+}$ in $Fe^{3+}AlO_3$-bearing Pv and PPv by X-ray emission spectroscopy (XES) and X-ray diffraction (XRD) in a laser-heated diamond anvil cell (DAC). These Al-bearing starting materials were chosen because the lower mantle contains Al as well as iron as secondary component, and recent studies indicate that $Fe^{3+}$ is more dominant than $Fe^{2+}$ and that $Fe^{3+}$-Al coupled substitution occurs in Al-bearing Pv (Frost et al., 2004; McCammon, 2005; Nishio-Hamane

* Corresponding author. Tel.: +81 89 927 8151; fax: +81 89 927 8167.
*E-mail address:* fujino@sci.ehime-u.ac.jp (K. Fujino).

0031-9201/$ - see front matter © 2013 Elsevier B.V. All rights reserved.
http://dx.doi.org/10.1016/j.pepi.2013.12.008

et al., 2005). Our results on Pv and PPv were separately reported in Fujino et al. (2012) and Fujino et al. (2013), respectively.

In this paper, we summarize our results on the spin transitions and substitutions of $Fe^{3+}$ in Al-bearing Pv and PPv, focusing on the similarities and dissimilarities between Al-bearing Pv and PPv. Then, combining these results on $Fe^{3+}$ with the recent first-principles calculations on the spin state of $Fe^{2+}$ in Pv and PPv, the spin transition and substitution of iron in pyrolitic lower mantle minerals are proposed. Finally, their effects on iron-partitioning among the lower mantle minerals are discussed.

## 2. Experimental procedure

The Pv and PPv samples used for the XES and XRD measurements were synthesized from gel with the composition of $Mg_{0.85}Fe^{3+}_{0.15}Al_{0.15}Si_{0.85}O_3$, which was previously heated at 1000 K in an open atmosphere to keep iron as $Fe^{3+}$. The Pv samples were synthesized at 25 GPa, 2000 K in a multi-anvil cell and loaded in a DAC, while the PPv samples were synthesized at 165–170 GPa (before heating), 2100 K directly in a DAC by laser-heating because the PPv samples are not pressure-quenchable.

XES and XRD measurements of the Pv samples (Syn2, Syn5, and Syn7) and PPv samples (F004 and F005) were carried out at beam lines BL-12XU and BL-10XU, respectively, at SPring-8. In the XES measurements, an incident X-ray beam of 11 keV was used and the emitted X-ray was measured from 7020 to 7080 eV. The energy resolution was approximately 0.8 eV. The XES measurements of the Pv samples were carried out up to 200 GPa at room temperature after annealing at 1200–1400 K at each pressure in most cases, while the XES measurements of the PPv samples were carried out at room temperature without annealing at each pressure during decompression from 165 to 37 GPa to prevent the phase transition to Pv. As the reference spectra of HS and LS states of $Fe^{3+}$, the XES spectra of $Fe^{3+}$ in powdered hematite $Fe_2O_3$ were also measured at pressures up to 79 GPa at room temperature. Throughout the experiments, pressures of the DACs at room temperature were determined by the shift of the Raman spectrum of diamond by the method of Akahama and Kawamura (2005) for consistency.

During the XES measurements, the XRD patterns of the samples were taken at selected pressures to confirm the phase and measure the cell parameters of the samples. Further experimental details and results for Pv and PPv are reported in Fujino et al. (2012) and Fujino et al. (2013), respectively. The summarized experimental conditions and the obtained results for Pv and PPv are given in Table 1. Here, the pressures except for the synthesis pressure of Mg-Pv were all measured at room temperature at which the XES measurements were carried out. Therefore, the pressures during annealing will be slightly higher than the respective pressures at room temperature by thermal pressures. The synthesis pressure (25 GPa at 2000 K) of Mg-Pv was calibrated from the in situ high P, T data of the similar experiments at SPring-8. The measured XES spectra of Pv and PPv are illustrated in Fig. 1 with the reference HS and LS spectra of $Fe_2O_3$. To estimate the HS ratios of $Fe^{3+}$ in respective samples, the observed XES spectra were fitted by the linear combination of the HS and LS spectra of $Fe_2O_3$ to obtain the least-squares sum of the intensity differences of the observed and simulated patterns (Fujino et al., 2012). The results are also summarized in Table 1 and plotted in Fig. 2.

**Table 1**
Experimental conditions and results.

| Sample (syn. P, T) | Pressure at 300 K (GPa)[a] | Phase by XRD[b] | Cell volume (Å$^3$) | High spin ratio by XES |
|---|---|---|---|---|
| *Mg-perovskite (25 GPa, 2000 K)* | | | | |
| Syn2 | 60*[c] | Pv | 141.9(8) | 0.77 |
| | 36 | | | 0.80 |
| Syn5 | 45* | | | 0.89 |
| | 0 | | | 0.91 |
| Syn7 | 120* | Pv | 127.7(3) | 0.80 |
| | 150* | | | 0.67 |
| | 165* | | | 0.63 |
| | 174 | Pv | 119.2(6) | |
| | 177 | | | 0.55 |
| | 200 | | | 0.51 |
| *Post-Mg-perovskite* | | | | |
| F004 (165 GPa, 2100 K) | 162* | PPv | 116.4(4) | 0.03 |
| | 138 | | | 0.02 |
| | 115 | | | 0.02 |
| | 90 | | | 0.0 |
| | 72 | PPv | 131.4(7) | 0.20 |
| | 49 | PPv | 151(7) | 0.32 |
| F005 (170 GPa, 2100 K) | 165* | PPv | 116.2(7) | 0.06 |
| | 126 | | | 0.06 |
| | 103 | | | 0.14 |
| | 107 | PPv | 123.7(4) | |
| | 78 | | | 0.15 |
| | 60 | | | 0.35 |
| | 37 | amor | | 0.50 |

[a] The pressures of the respective samples were varied from upper to lower with time. For Syn7, pressure changed from 165 to 174-177 GPa after an interval of half year without additional pressure increase of the DAC.
[b] Pv = Mg-perovskite, PPv = post-Mg-perovskite, amor = amorphous.
[c] Pressures with * mean that the sample was annealed or heated before the XES measurement at this pressure.

## 3. Results and discussion

### 3.1. Spin transition and substitution of $Fe^{3+}$ in $Fe^{3+}AlO_3$-bearing Pv and PPv

The XRD patterns of Pv and PPv samples showed single phase Pv and PPv, respectively, within the detection limit of XRD. These results indicate that Fe is all $Fe^{3+}$ and the coupled substitution, $Mg + Si \rightleftarrows Fe^{3+} + Al$, occurs in both Pv and PPv samples (Fujino et al., 2013), although the site occupancies of $Fe^{3+}$ and Al between the dodecahedral (A) and octahedral (B) sites are not fixed to the particular sites. The site occupancies of $Fe^{3+}$ and Al between the two cation sites in Pv and PPv were estimated from the spin state of $Fe^{3+}$ and the shift of the trend in the pressure–volume relations as described below.

With the spin state of $Fe^{3+}$ in Pv, the HS ratio of $Fe^{3+}$ (Fig. 2(a)) apparently seems to decrease gradually with pressure from around 50 GPa. However, the gradual decrease of HS ratio of $Fe^{3+}$ in Pv is considered to occur by the gradual $Fe^{3+}$–Al exchange reaction between the A- and B-sites, $^{HS}Fe^{3+}$(A-site) + Al(B-site) $\rightleftarrows$ Al(A-site) + $^{LS}Fe^{3+}$(B-site) (the superscripts HS and LS mean HS and LS states of $Fe^{3+}$), by annealing at low temperature of 1200–1400 K (Fujino et al., 2012). This is supported by the following two lines of evidence. Firstly, the recent experimental study (Catalli et al., 2010a) and first-principles calculations (Hsu et al., 2011) on $Fe_2O_3$-bearing Pv revealed that $Fe^{3+}$ equally enters the A- and B-sites and $Fe^{3+}$ at the A-site remains HS at lower mantle pressures, while $Fe^{3+}$ at the B-site undergoes the HS–LS transition between 50 and 60 GPa (Catalli et al., 2010a) or 40–70 GPa (Hsu et al., 2011). Further, Catalli et al. (2011) reported a rapid increase of LS $Fe^{3+}$ at the B-site near 70 GPa in Al-bearing Pv based on synchrotron Mössbauer spectroscopy (SMS) and XES. Secondly, the trends of the pressure–volume relations of our samples are different between the samples annealed at different temperatures (Fig. 3). Our previous samples synthesized at 75–117 GPa, 1600–2000 K from the same gel as our present samples, and annealed at 1600 K at each pressure, revealed the change of the trend of cell volume at 50–70 GPa (although the NaCl scale by Sata et al.,

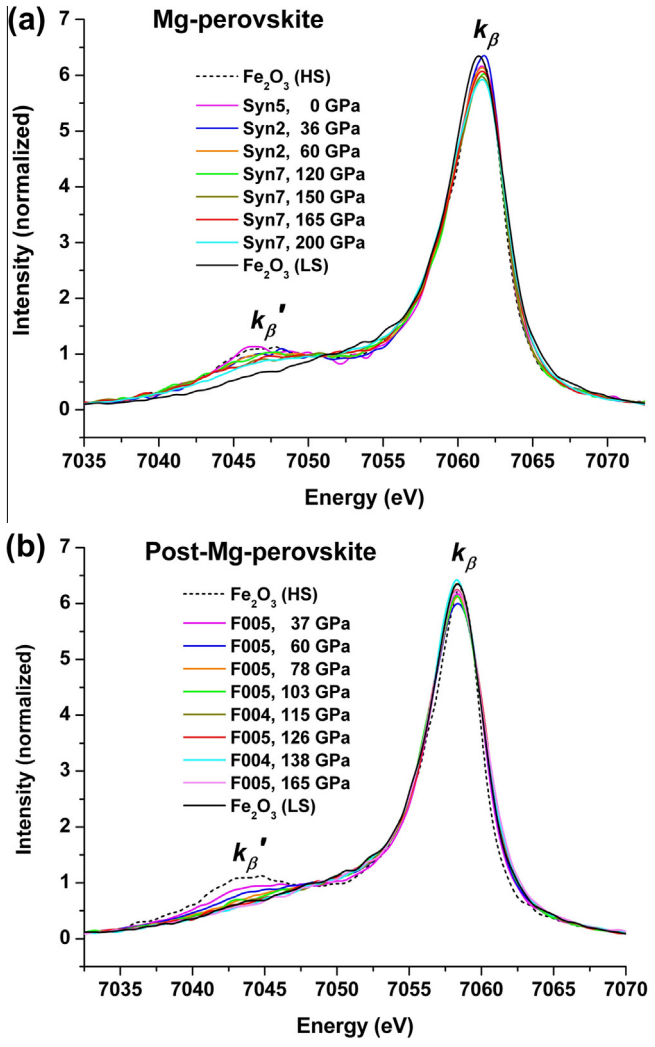


**Fig. 1.** X-ray emission spectra of (a) Pv and (b) PPv at room temperature. The intensities are background-subtracted by the line connecting the averaged counts at 7020 and 7080 eV and normalized so that the integrated areas from 7020 to 7080 eV become 100. The energies of $k_\beta$ peaks of the spectra of Pv and PPv are aligned with that of Syn5 at 0 GPa and that of F005 at 37 GPa, respectively, for comparison. The HS and LS spectra of $Fe_2O_3$ (black) are also plotted. The error bars of the data points are nearly double of the widths of the lines in most cases.

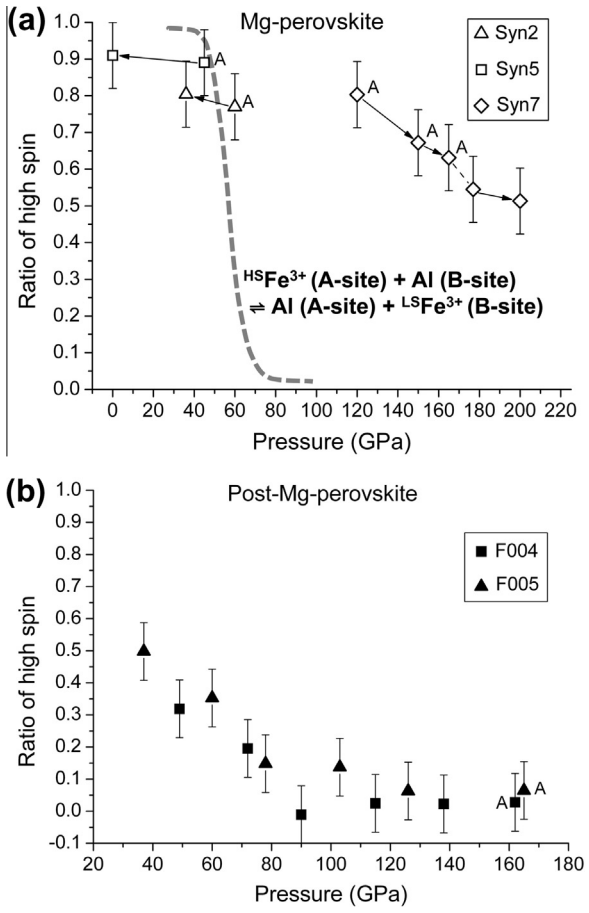


**Fig. 2.** The high spin ratios of $Fe^{3+}$ in (a) Pv and (b) PPv with pressure. The high spin ratios were estimated from the least-squares fitting of the XES spectra of $Fe^{3+}$ by the linear combination of HS and LS spectra of $Fe_2O_3$. The character A beside a data point indicates that the sample was annealed or heated at that pressure before the XES measurements. The bold dashed line in (a) indicates that the $Fe^{3+}$–Al exchange reaction between the A- and B-sites at high enough temperature occurs along this line.

2002, is used here, it is nearly the same with the diamond scale by Akahama and Kawamura, 2005, at these pressure region), indicating the occurrence of the above $Fe^{3+}$–Al exchange reaction between the A- and B-sites at these pressures. Hsu et al. (2011) also reported the cell volume reduction at 45–60 GPa by the HS–LS transition of $Fe^{3+}$ at the B-site in $Fe_2O_3$-bearing Pv. From the above two reasons $Fe^{3+}$ in our Pv is considered to occupy the A-site and is HS just after the synthesis at 25 GPa and 2000 K and below ~50 GPa, but between 50 and 70 GPa $Fe^{3+}$ replaces Al at the B-site and becomes LS with pressure along the path of the dashed line in Fig. 2(a) when the samples are annealed at temperatures high enough to promote the $Fe^{3+}$–Al exchange reaction. However, in Fig. 3 our present samples annealed at 1200–1400 K lie on the upper trend of the cell volume below 50 GPa but above 70 GPa they still lie nearly on the extension of the upper trend of the cell volume. This can be interpreted that above 50–70 GPa $Fe^{3+}$ in our present samples gradually replaces Al at the B-site and becomes LS by successive low temperature anealings. In Fujino et al. (2012), we reported that the $Fe^{3+}$-Al exchange reaction between the A- and B-sites in Pv occurs between 50–60 GPa. However, from Fig. 3, it will be better to consider that the $Fe^{3+}$–Al exchange reaction in Pv occurs between 50 and 70 GPa.

These results reveal the important point that the spin state of $Fe^{3+}$ in Pv is not simply defined by pressure and temperature of the spin state measurements but also definitely affected by cation distributions between the A- and B-sites, and these cation distributions are strongly controlled by the synthesis and annealing conditions of the samples. This can be also applied to PPv, because Pv and PPv have two cation sites, A and B. This is the largely different point from the case of ferropericlase which has only one cation site. This means that the spin state of $Fe^{3+}$ of the same Pv sample shows the different spin state even at the same pressure and temperature, depending on the synthesis and annealing conditions of the sample before the spin state measurement. This explains the large conflict of the previous reports why the spin states of $Fe^{3+}$ in Pv samples with the similar composition differ with each other at the similar P, T conditions. The careful analyses of the synthesis and annealing conditions of those samples will resolve the conflict among them.

Meanwhile in PPv (Fig. 2(b)), $Fe^{3+}$ is fully LS above ~100 GPa, and begins to significantly change from LS to HS below ~80 GPa during decompression without annealing. Before these results (Fujino et al., 2013) there was no experimental report on the spin state of $Fe^{3+}$ in Al-bearing PPv. Catalli et al. (2010b) reported the nearly equal occupancies of HS $Fe^{3+}$ at the A-site and LS $Fe^{3+}$ at the B-sites for 128–138 GPa in $Fe_2O_3$-bearing PPv. First-principles

Please cite this article in press as: Fujino, K., et al. Spin transition, substitution, and partitioning of iron in lower mantle minerals. Phys. Earth Planet. In. (2014), http://dx.doi.org/10.1016/j.pepi.2013.12.008

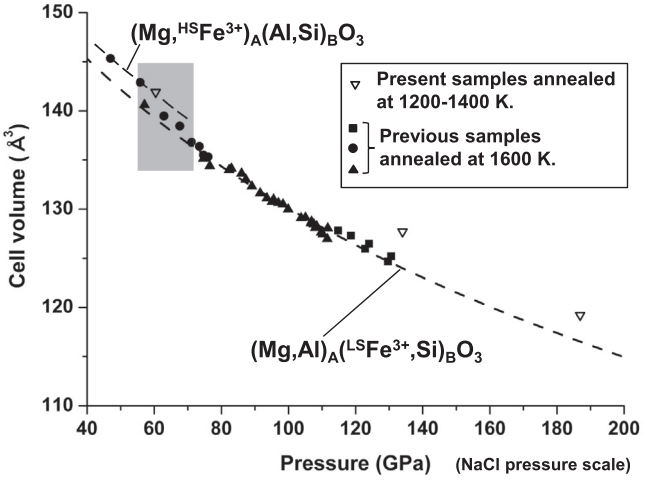


**Fig. 3.** Pressure–volume relations of the Pv samples annealed at different temperatures. Here, pressure is scaled by NaCl (Sata et al., 2002) because NaCl was the only pressure marker common to all the samples. The present samples (open triangles) were synthesized at 25 GPa, 2000 K, and annealed at 1200–1400 K at each pressure. The previous samples (samples in Nishio-Hamane et al., 2008 and samples added later) (closed symbols) were synthesized at 75–117 GPa, 1600–2000 K from the same gel as the present samples, and annealed at 1600 K at each pressure. The lower dashed regression line was approximated by the 3rd Birch-Murnaghan equation of state using the data points of closed symbols above 70 GPa, and is considered to correspond to the (Mg, Al)$_A$($^{LS}$Fe$^{3+}$, Si)$_B$O$_3$ configuration. The upper dashed line, which passes through the data points of closed symbols below ~55 GPa and is considered to correspond to the (Mg, $^{HS}$Fe$^{3+}$)$_A$(Al, Si)$_B$O$_3$ configuration, is drawn as a guide for the eye.

calculations (Yu et al., 2012) also predicted the same occupancies of HS $Fe^{3+}$ at the A-site and LS $Fe^{3+}$ at the B-site for $Fe_2O_3$-bearing PPv. From these results, LS $Fe^{3+}$ in our PPv samples is considered to occupy the B-site at the synthesis condition, 165–170 GPa and 2100 K. This cation configuration of Al at the A-site and LS $Fe^{3+}$ at the B-site is considered to continue as the favorable cation distribution of $Fe^{3+}AlO_3$-bearing PPv between 165 and 100 GPa (Fujino et al., 2013) because the cell volumes of the PPv samples synthesized from the same gel as ours, and annealed at 1600 K at each pressure (Nishio-Hamane and Yagi, 2009, Fig. 2), do not show a change of the trend of cell volumes, as observed in Fig. 3, in the pressure–volume curve between 110 and 165 GPa.

The comparison of the spin transitions and substitutions of $Fe^{3+}$ between our $Fe^{3+}AlO_3$-bearing Pv and PPv indicates that the coupled substitution, Mg + Si ⇄ $Fe^{3+}$ + Al, is working in both Pv and PPv, and Pv above 70 GPa and PPv above 80–100 GPa have the same cation configuration, Al at the A-site and LS $Fe^{3+}$ at the B-site, as the stable or favorable cation configuration. The $Fe^{3+}$–Al exchange reaction between the A- and B-sites in Pv above 50–70 GPa, which is induced by the HS–LS transition of $Fe^{3+}$, only occurs at high temperature. Therefore, the HS–LS transition pressure of $Fe^{3+}$ at the B-site in our Pv at room temperature will be below 50–70 GPa, assuming the positive Clapeyron slope of the HS–LS transition of $Fe^{3+}$. This is slightly lower than that in PPv (below ~80 GPa).

### 3.2. Spin transition and substitution of iron in lower mantle minerals

Now we consider the spin transition and substitution of iron in lower mantle minerals. Here, we consider the pyrolite composition for the lower mantle, where the dominant iron-bearing phases are Fp, Pv, and PPv. With the chemistry of Fp, it can be approximated as (Mg, $Fe^{2+}$)O, although some other minor elements will be present in Fp. With the chemistries of Pv and PPv, the analyzed compositions of synthesized Pv and PPv of the pyrolite composition (Irifune et al., 2010; Sinmyo et al., 2011) indicate that $MgSiO_3$ Pv and PPv are substituted by Fe and Al (Fe ≈ Al for Pv and Fe < Al for PPv). Also, $Fe^{3+}$ is considered to be more dominant than $Fe^{2+}$ in Pv (Frost et al., 2004; McCammon, 2005). Therefore, Pv and PPv in pyrolitic lower mantle can be approximated as the solid solutions of $MgSiO_3$, $Fe^{2+}SiO_3$, $Fe^{3+}AlO_3$, and $Al_2O_3$.

Our experimental studies clarified the spin transition behaviors of $Fe^{3+}$ in Al-bearing Pv and PPv. With the spin transition behaviors of $Fe^{2+}$ in Pv and PPv, the recent experimental results and first-principles calculations indicate that $Fe^{2+}$ always occupies the A-site and remains HS at the lower mantle conditions both in Pv (Hsu et al., 2010, 2011; Lin et al., 2012) and PPv (Yu et al., 2012). Combining our experimental results on the spin transitions of $Fe^{3+}$ in Al-bearing Pv and PPv with the above recent studies on the spin transitions of $Fe^{2+}$ in Pv and PPv, and further combining the previous reports on Fp (Badro et al., 2003; Lin et al., 2005; Speziale et al., 2005), we can figure out the spin transitions of iron in iron-bearing lower mantle minerals as illustrated in Fig. 4. For Fp, virtually it contains only $Fe^{2+}$ and it changes from HS to LS between 40 and 80 GPa. For Pv, $Fe^{2+}$ occupies the A-site and remains HS for the whole lower mantle, while $Fe^{3+}$ occupies the A-site and is HS at pressures below ~50 GPa. Then, between 50 and 70 GPa, $Fe^{3+}$ at the A-site replaces Al at the B-site and becomes LS. Meanwhile, for PPv, $Fe^{2+}$ is always at the A-site and HS and $Fe^{3+}$ is always at the B-site and LS for the whole range of lowermost mantle pressures. The Clapeyron slopes of spin transitions of iron in lower mantle minerals are not exactly considered in constructing Fig. 4, although they are generally considered to be small. However, Fig. 4 is illustrated based on the cation exchange reactions in Pv and PPv which can occur only at high temperature. Therefore, the spin states of iron in Pv and PPv in Fig. 4 are not at room temperature but at high temperature where the cation exchange reactions can proceed.

### 3.3. Effects of spin transition and substitution of iron on iron-partitioning among the lower mantle minerals

Iron-partitioning among the iron-bearing lower mantle minerals are largely affected by the spin transition and substitution of iron in lower mantle minerals. In the following, we discuss how the iron-partitioning between Pv and Fp, and PPv and Fp in the lower mantle are affected by the spin transition and substitution of iron in lower mantle minerals. Here again, we consider the pyrolite composition as the model for the lower mantle. Fig. 5 summarizes the partition coefficient $K_D$ of Fe–Mg between coexisting Pv and Fp, and PPv and Fp in the previous reports of the pyrolite composition as a function of pressure, where $K_D = (Fe/Mg)_{Pv}/(Fe/Mg)_{Fp}$ or $(Fe/Mg)_{PPv}/(Fe/Mg)_{Fp}$ (Fe includes both $Fe^{2+}$ and $Fe^{3+}$). Although the data points of $K_D$ are scattered, a steep increase at 23–30 GPa and a steep decrease at 40–60 GPa can be generally recognized below ~90 GPa. However, above ~90 GPa there seem two trends in

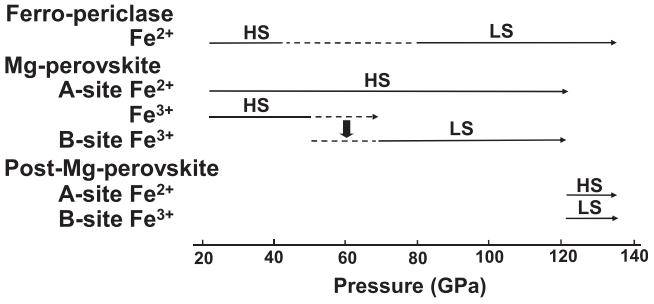


**Fig. 4.** The schematic drawing of the estimated spin states of iron in pyrolitic lower mantle minerals.

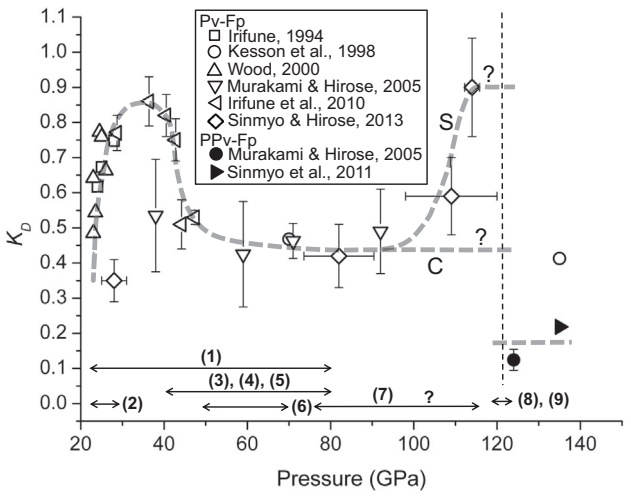


**Fig. 5.** Variations of $K_D = (Fe/Mg)_{Pv}/(Fe/Mg)_{Fp}$ or $(Fe/Mg)_{PPv}/(Fe/Mg)_{Fp}$ with pressure in pyrolitic lower mantle. Fe includes both $Fe^{2+}$ and $Fe^{3+}$. The two trends C and S are drawn above 90 GPa. The labels (1) to (9) given to the pressure intervals at the bottom of the figure refer to the possible reaction equations in the text, and the pressure intervals indicate the regions where the respective reactions would be taking place. The $K_D$ data are from Irifune (1994), Kesson et al. (1998), Wood (2000), Murakami and Hirose (2005), Irifune et al. (2010), Sinmyo et al. (2011), and Sinmyo and Hirose (2013).

Fig. 5. One is nearly constant with pressure till the Pv–PPv boundary (denoted as C in Fig. 5), and the other a steep increase toward the Pv–PPv boundary (denoted as S in Fig. 5). Further, the discontinuous change of $K_D$ is recognized at the Pv–PPv boundary, although the data is very limited.

In Fig. 5, the numbers with a parenthesis and the pressure intervals at the lower part of the figure are the possible reactions, which are given in the text, and their pressure intervals where those reactions mainly work. The following exchange reaction of HS $Fe^{2+}$ and Mg between Pv and Fp without the spin transition of iron is considered to be working at the upper part of the lower mantle.

$$^{HS}Fe^{2+}SiO_3(Pv) + MgO(Fp) \rightarrow {}^{HS}Fe^{2+}O(Fp) + MgSiO_3(Pv) \quad (1)$$

However, the steep changes of $K_D$ at 23–30 GPa and 40–60 GPa seem to be difficult to be explained by Eq. (1). We think that the steep increase of $K_D$ at 23–30 GPa in Fig. 5 can be interpreted to occur by the following valence disproportionation reaction of HS $Fe^{2+}$.

$$3^{HS}Fe^{2+}O(Fp,\ Mj) + Al_2O_3(Mj) \rightarrow 2^{HS}Fe^{3+}AlO_3(Pv) + \text{Fe-metal} \quad (2)$$

where Mj denotes majorite $(Mg, Fe^{2+}, Ca)_3(Mg, Fe^{2+}, Al, Si)_2Si_3O_{12}$ which coexists with Pv, Fp, and Ca-perovskite in the uppermost part of the lower mantle (Irifune, 1994). In the above equation, most of $^{HS}Fe^{2+}O$ in the left side is supplied from coexisting Fp because the Fe/Mg ratio of coexisting Mj is much lower than that of Pv (Irifune, 1994). The increase of the solubility limit of $Fe^{3+}AlO_3$ component in Pv with pressure (Nishio-Hamane et al., 2005) may also enhance the steep increase of iron in Pv in Fig. 5. Meanwhile, the steep decrease of $K_D$ at 40–60 GPa is considered to be induced by the HS–LS transition of $Fe^{2+}$ in Fp,

$$^{HS}Fe^{2+}O(Fp) \rightarrow {}^{LS}Fe^{2+}O(Fp) \quad (3)$$

and the following two reactions will proceed because both $Fe^{2+}$ and $Fe^{3+}$ in Pv decrease in this pressure region (Irifune et al., 2010).

$$^{HS}Fe^{2+}SiO_3(Pv) + MgO(Fp) \rightarrow {}^{LS}Fe^{2+}O(Fp) + MgSiO_3(Pv) \quad (4)$$

$$2^{HS}Fe^{3+}AlO_3(Pv) + \text{Fe-metal} \rightarrow 3^{LS}Fe^{2+}O(Fp) + Al_2O_3(Pv) \quad (5)$$

Eq. (4) is the $Fe^{2+}$–Mg exchange reaction between Pv and Fp, where the HS–LS transition of $Fe^{2+}$ accompanies. Eq. (5) is the reverse reaction of valence disproportionation reaction (2), but HS $Fe^{3+}$ changes to LS $Fe^{2+}$ and $Al_2O_3$ is preserved in Pv, differently from Eq. (2), because Mj which would play a host for $Al_2O_3$ disappears at these pressures. Between 50 and 70 GPa, the remaining HS $Fe^{3+}$ at the A-site in Pv will become LS $Fe^{3+}$ at the B-site by the following $Fe^{3+}$–Al exchange reaction between the A- and B-sites.

$$^{HS}Fe^{3+}AlO_3(Pv) \rightarrow Al^{LS}Fe^{3+}O_3(Pv) \quad (6)$$

However, the effect of this reaction on $K_D$, which alone would increase $K_D$, will become inconspicuous due to the overlapping with the reactions (4) and (5), both of which decrease $K_D$. The trend C may be explained by the above reactions.

With the case of trend S in Fig. 5, Sinmyo et al. (2011) raised two possibilities for the cause of $K_D$ increase with pressure; one is the effect of HS–LS transition of $Fe^{3+}$ in Pv, and the other the effect of temperature and/or pressure. In the former case, the following reaction needs to occur above 90 GPa to increase $K_D$.

$$3^{LS}Fe^{2+}O(Fp) + Al_2O_3(Pv) \rightarrow 2Al^{LS}Fe^{3+}O_3(Pv) + \text{Fe-metal} \quad (7)$$

The reaction (7) is the valence disproportionation reaction of LS iron, and does not involve the HS–LS transition of iron. In this case, the reaction (7) is induced by reaction (6) above 90 GPa. However, the spin transition of $Fe^{3+}$ in Pv above 90 GPa is inconsistent with our case (between 50 and 70 GPa) or Catalli et al. (2011) (near 70 GPa), and the realization of reaction (7) at such high pressure seems difficult. At still higher pressures above Pv–PPv bounrdary, PPv has no spin transition with both $Fe^{2+}$ and $Fe^{3+}$ within its stability region. However, there may be some drastic change of the amounts of HS and LS irons across the Pv–PPv boundary, if $K_D$ between PPv and Fp is much lower than that between Pv and Fp (Murakami and Hirose, 2005; Sinmyo et al., 2011) as illustrated in Fig. 5. In this case, the following reactions will occur across the Pv–PPv boundary.

$$^{HS}Fe^{2+}SiO_3(Pv) + MgO(Fp) \rightarrow {}^{LS}Fe^{2+}O(Fp) + MgSiO_3(PPv) \quad (8)$$

$$2Al^{LS}Fe^{3+}O_3(Pv) + \text{Fe-metal} \rightarrow 3^{LS}Fe^{2+}O(Fp) + Al_2O_3(PPv) \quad (9)$$

Therefore, it is expected by these reactions that HS $Fe^{2+}$ and LS $Fe^{3+}$ in PPv are much lower than those in Pv, and LS $Fe^{2+}$ in Fp increases across the Pv–PPv boundary. To establish the reaction scheme to explain the iron-partitioning between Pv–Fp and PPv–Fp with pressure, further experimental studies on iron-partitioning with the reliable analyses of the valence and spin states of Fe in coexisting Pv and Fp, and PPv and Fp are required.

## 4. Summary

Our experimental studies revealed that the spin state of $Fe^{3+}$ in Al-bearing Pv and PPv deeply depends on which site $Fe^{3+}$ occupies between the A- and B-sites, and the site occupancies of $Fe^{3+}$ between these two sites are strongly controlled by the synthesis and annealing conditions of the samples. Most of the large discrepancies in the previous reports on the spin transition of $Fe^{3+}$ may likely be attributed to the approaches to the spin transition problems of $Fe^{3+}$ in the previous studies, where much attention was not paid to the above points. The combination of the present experimental studies on $Fe^{3+}$ and recent first-principles calculations on $Fe^{2+}$ has a high possibility to resolve the spin transition problems of iron in Pv and PPv in the previous reports. To clarify the kinetics of $Fe^{3+}$–Al exchange reaction between the A- and B-sites and confirm the relation between the spin state of $Fe^{3+}$ and the occupied site by direct structure analysis will be the next targets. Our model of the spin transitions and substitutions of iron in pyrolitic lower

Please cite this article in press as: Fujino, K., et al. Spin transition, substitution, and partitioning of iron in lower mantle minerals. Phys. Earth Planet. In. (2014), http://dx.doi.org/10.1016/j.pepi.2013.12.008

mantle minerals explains the basic points of the iron-partitioning among the iron-bearing lower mantle minerals in the previous reports. However, to better understand the iron-partitioning among the iron-bearing lower mantle minerals, further high pressure phase equilibrium experiments of pyrolitic composition and reliable analyses of the valence and spin states of iron in the coexisting iron-bearing phases are required.

## Acknowledgements

We thank N. Hiraoka, H. Ishii, and K.-D. Tsuei at NSRRC, and Y. Ohishi at Spring-8 for their help in the X-ray emission and X-ray diffraction experiments, respectively. We also thank two anonymous reviewers to improve the manuscript. This work was supported by the Grant-in-Aid (No. 21540491) by the Japan Society for the Promotion of Science (JSPS). The X-ray emission spectroscopy experiments were performed under the approvals of NSRRC (Proposal Nos. 2007-2-033-1, 2007-2-033-2, 2007-2-033-4, 2008-3-032-2, No. 2008-3-032-5, and 2008-3-032-6) and JASRI (Nos. 2007A4261, 2007B4254, 2008A4266, 2008B4263, No. 2009B4267, and 2010A4251), while the X-ray diffraction experiments were carried out under the approval of JASRI (Nos. 2007A1604, 2007B1547, 2008A1559, 2008B1311, Nos. 2009B1080, and 2010A1545).

## References

Akahama, Y., Kawamura, H., 2005. Raman study on the stress state of [111] diamond anvils at multimegabar pressure. J. Appl. Phys. 98, 083523 (1–4).

Andrault, D., Munoz, M., Bolfan-Casanova, N., Guignot, N., Perrillat, J.-P., Aquilanti, G., Pascarelli, S., 2010. Experimental evidence for perovskite and post-perovskite coexistence throughout the whole D″ region. Earth Planet. Sci. Lett. 293, 90–96.

Badro, J., Fiquet, G., Guyot, F., Rueff, J.P., Struzhkin, V.V., Vanko, G., Monaco, G., 2003. Iron partitioning in Earth's mantle: toward a deep lower mantle discontinuity. Science 300, 789–791.

Badro, J., Rueff, J.-P., Vanko, G., Monaco, G., Fiquet, G., Guyot, F., 2004. Electronic transitions in perovskite: possible nonconvecting layers in the lower mantle. Science 305, 383–386.

Bengtson, A., Li, J., Morgan, D., 2009. Mössbauer modeling to interpret the spin state of iron in (Mg, Fe)$SiO_3$ perovskite. Geophys. Res. Lett. 36, L1531 (doi:10.1029/2009GL038340).

Catalli, K., Shim, S.-H., Prakapenka, V.B., Zhao, J., Struhahn, W., Chow, P., Xiao, Y., Liu, H., Cynn, H., Evans, W.J., 2010a. Spin state of ferric iron in $MgSiO_3$ perovskite and its effect on elastic properties. Earth Planet. Sci. Lett. 289, 68–75.

Catalli, K., Shim, S.-H., Prakapenka, V.B., Zhao, J., Struhahn, W., 2010b. X-ray diffraction and Mössbauer spectroscopy of $Fe^{3+}$-bearing Mg-silicate post-perovskite at 128–138 GPa. Am. Miner. 95, 418–421.

Catalli, K., Shim, S.-H., Dera, P., Prakapenka, V.B., Zhao, J., Struhahn, W., Chow, P., Xiao, Y., Cynn, H., Evans, W.J., 2011. Effects of the $Fe^{3+}$ spin transition on the properties of aluminous perovskite–New insights for lower-mantle seismic heterogeneities. Earth Planet. Sci. Lett. 310, 293–302. http://dx.doi.org/10.1016/j.epsl.2011.08.018.

Frost, D.J., Liebske, C., Langenhorst, F., McCammon, C.A., Tronnes, R.G., Rubie, D.C., 2004. Experimental evidence for the existence of iron-rich metal in the Earth's lower mantle. Nature 428, 409–412.

Fujino, K., Nishio-Hamane, D., Seto, Y., Sata, N., Nagai, T., Shinmei, T., Irifune, T., Ishii, H., Hiraoka, N., Cai, Y.-Q., Tsuei, K.-D., 2012. Spin transition of ferric iron in Al-bearing Mg-perovskite up to 200 GPa and its implication for the lower mantle. Earth Planet. Sci. Lett. 317–318, 407–412. http://dx.doi.org/10.1016/j.epsl.2011.12.006.

Fujino, K., Nishio-Hamane, D., Kuwayama, Y., Sata, N., Murakami, S., Whitaker, M.L., Shinozaki, A., Ohfuji, H., Kojima, Y., Irifune, T., Hiraoka, N., Ishii, H., Tsuei, K.-D., 2013. Spin transition and substitution of $Fe^{3+}$ in Al-bearing post-Mg-perovskite. Phys. Earth Planet. Inter. 217, 31–35. http://dx.doi.org/10.1016/j.pepi.2013.01.006.

Hsu, H., Umemoto, K., Blaha, P., Wentzcovitch, R.M., 2010. Spin states and hyperfine interactions of iron in (Mg, Fe)$SiO_3$ perovskite under pressure. Earth Planet. Sci. Lett. 294, 19–26. http://dx.doi.org/10.1016/j.epsl.2010.02.031.

Hsu, H., Blaha, P., Cococcini, M., Wentzcovitch, R.M., 2011. Spin-state crossover and hyperfine interactions of ferric iron in $MgSiO_3$ perovskite. Phys. Rev. Lett. 106, 118501. http://dx.doi.org/10.1103/PhysRevLett. 106.118501.

Irifune, T., 1994. Absence of an aluminous phase in the upper part of the Earth's lower mantle. Nature 370, 131–133.

Irifune, T., Shinmei, T., McCammom, C.A., Miyajima, N., Rubie, D.C., Frost, D.J., 2010. Iron partitioning and density changes of pyrolite in Earth's lower mantle. Science 327, 193–195. http://dx.doi.org/10.1126/science.1181443.

Jackson, J.M., Struhahn, W., Shen, G., Zhao, J., Hu, M.Y., Errandonea, D., Bass, J.D., Fei, Y., 2005. A synchrotron Mössbauer spectroscopy study of (Mg, Fe)$SiO_3$ perovskite up to 120 GPa. Am. Miner. 90, 199–205.

Jackson, J.M., Struhahn, W., Tschauner, O., Lerche, M., Fei, Y., 2009. Behavior of iron in (Mg, Fe)$SiO_3$ post-perovskite assemblages at Mbar pressures. Geophys. Res. Lett. 36, L10301. http://dx.doi.org/10.1029/2009GL037815.

Kesson, S.E., Fitz Gerald, J.D., Shelley, J.M., 1998. Mineralogy and dynamics of a pyrolite lower mantle. Nature 393, 252–255.

Li, L., Brodholt, J.P., Stackhouse, S., Weidner, D.J., Alfredsson, M., Price, G.D., 2005. Electronic spin state of ferric iron in Al-bearing perovskite in the lower mantle. Geophys. Res. Lett. 32, L17307.

Li, J., Sturhahn, W., Jackson, J.M., Struzhkin, V.V., Lin, J.F., Zhao, J., Mao, H.K., Shen, G., 2006. Pressure effect on the electronic structure of iron in (Mg, Fe) (Si, Al)$O_3$ perovskite: a combined synchrotron Mossbauer and X-ray emission spectroscopy study up to 100 GPa. Phys. Chem. Miner. 33, 575–585.

Lin, J.F., Struzhkin, V.V., Jacobsen, S.D., Hu, M.Y., Chow, P., Kung, J., Liu, H., Mao, H.K., Hemley, R.J., 2005. Spin transition of iron in magnesiowüstite in the Earth's lower mantle. Nature 436, 377–380.

Lin, J.F., Watson, H., Vanko, G., Alp, E.E., Prakapenka, V.B., Dera, P., Struzhkin, V.V., Kubo, A., Zhao, J., MacCammon, C., Evans, W.J., 2008. Intermediate-spin ferrous iron in lowermost mantle post-perovskite and perovskite. Nat. Geosci. 1, 688–691.

Lin, J.F., Alp, E.E., Mao, Z., Inoue, T., McCammon, C., Xiao, Y., Chow, P., Zhao, J., 2012. Electronic spin states of ferric and ferrous iron in the lower-mantle silicate perovskite. Am. Miner. 97, 592–597.

McCammon, C., 2005. The paradox of mantle redox. Science 308, 807–808.

McCammon, C., Kantor, I., Narygina, O., Rouquette, J., Ponkratz, U., Sergueev, I., Mezouar, M., Prakapenka, V., Dubrovinsky, L., 2008. Stable intermediate-spin ferrous iron in lower-mantle perovskite. Nat. Geosci. 1, 684–687.

McCammon, C., Dubrovinsky, L., Narygina, O., Kantor, I., Wu, X., Glazyrin, K., Sergueev, I., Chumakov, A.I., 2010. Low-spin $Fe^{2+}$ in silicate perovskite and a possible layer at the base of the lower mantle. Phys. Earth Planet. Inter. 180, 215–221.

Murakami, M., Hirose, K., Kawamura, K., Sata, N., Ohishi, Y., 2004. Post-perovskite phase transition in MgSiO3. Science 304, 855–858.

Murakami, M., Hirose, K., 2005. Post-perovskite phase transition and mineral chemistry in the pyrolitic lowermost mantle. Geophys. Res. Lett. 32, L03304. http://dx.doi.org/10.1029/2004GL021956.

Nishio-Hamane, D., Nagai, T., Fujino, K., Seto, Y., Takafuji, N., 2005. $Fe^{3+}$ and Al solubilities in $MgSiO_3$ perovskite: implication of the $Fe^{3+}AlO_3$ substitution in $MgSiO_3$ perovskite at the lower mantle condition. Geophys. Res. Lett. 32, L16306. http://dx.doi.org/10.1029/2005GL023529.

Nishio-Hamane, D., Seto, Y., Fujino, K., Nagai, T., 2008. Effect of $FeAlO_3$ incorporation into $MgSiO_3$ on the bulk modulus of perovskite. Phys. Earth Planet. Inter. 166, 219–225. http://dx.doi.org/10.1016/j.pepi.2008.01.002.

Nishio-Hamane, D., Yagi, T., 2009. Equations of state for postperovskite phases in the $MgSiO_3$–$FeSiO_3$–$FeAlO_3$ system. Phys. Earth Planet. Inter. 175, 145–150.

Sata, N., Shen, G., Rivers, M.L., Sutton, S.R., 2002. Pressure-volume equation of state of the high-pressure B2 phase of NaCl. Phys. Rev. B 65, 104114 (1–7).

Sinmyo, R., Hirose, K., Muto, S., Ohishi, Y., Yasuhara, A., 2011. The valence state and partitioning of iron in the Earth's lowermost mantle. J. Geophys. Res. 116, B07205. http://dx.doi.org/10.1029/2010JB008179.

Sinmyo, R., Hirose, K., 2013. Iron partitioning in pyrolitic lower mantle. Phys. Chem. Miner. 40, 107–113. http://dx.doi.org/10.1007/s00269-0551-7.

Speziale, S., Milner, A., Lee, V.E., Clark, S.M., Pasternak, M.P., Jeanloz, R., 2005. Iron spin transition in Earth's mantle. Proc. Natl. Acad. Sci. USA 102, 17918–17922.

Stackhouse, S., Brodholt, J.P., Price, G.D., 2007. Electronic spin transitions in iron-bearing $MgSiO_3$ perovskite. Earth Planet. Sci. Lett. 253, 282–290.

Yu, Y.G., Hsu, H., Cococcioni, M., Wentzcovitch, R.M., 2012. Spin states and hyperfine interactions of iron incorporated in $MgSiO_3$ post-perovskite. Phys. Earth Planet. Inter. 331–332, 1–7.

Zhang, F., Oganov, A.R., 2006. Valence state and spin transitions of iron in Earth's mantle silicates. Earth Planet. Sci. Lett. 249, 436–443.

Wood, B.J., 2000. Phase transformations and partitioning relations in peridotite under lower mantle conditions. Earth Planet. Sci. Lett. 174, 341–354.

Please cite this article in press as: Fujino, K., et al. Spin transition, substitution, and partitioning of iron in lower mantle minerals. Phys. Earth Planet. In. (2014), http://dx.doi.org/10.1016/j.pepi.2013.12.008